

Shell filling in non-linear magneto-tunneling spectroscopy of vertical quantum dots

B. Jouault¹, G. Faini^{*1}, A. Angelucci², M. Di Stasio², G. Santoro³, A. Tagliacozzo², F. Laruelle¹, R. Werner⁴, A. Forchel⁴

¹ *L2M-CNRS, 196 Avenue H. Ravéra, BP107, F-92225 Bagneux Cedex, France*

² *INFM and Università di Napoli "Federico II", Mostra d'Oltremare, Pad. 19, I-80125 Napoli, Italy*

³ *S.I.S.S.A. and INFM, Via Beirut 2-4, I-34013 Trieste, Italy*

⁴ *Technische Physik, Universität Würzburg, Am Hubland, D-97074 Würzburg, Germany*

**e-mail: giancarlo.faini@L2M.CNRS.fr*

We report on non-linear magneto-tunneling experiments carried out in single GaAs vertical quantum dots. We show that conduction at low voltage bias can be a spectroscopic tool for both the ground state and first excited states of few electrons on the dot. Increasing voltage a large resonant peak is observed and attributed to tunneling across the quasi-continuum of higher excited states.

Vertical quantum dots (QDs) obtained on double barrier resonant tunneling heterostructures better than those realized on lateral 2DEG systems allow to investigate the few electrons limit by starting from an empty dot and progressively charging it. However linear transport experiments require the addition of a lateral gate around the dots: the fabrication of such devices is a real technical difficulty and only few realizations have been reported in the literature till now [1].

We report here on new results in electron spectroscopy of more conventional two-contacted vertical QDs without a lateral gate. These structures are relatively easier to fabricate, but the theoretical analysis is difficult because transport is non-linear.

Coulomb staircase has been observed in these structures up to now only in presence of a strong barrier-thickness asymmetry [2,3]: when the electrons enter the QD from the thin barrier side, charge accumulation with subsequent electron-electron interaction is enhanced. *Viceversa*, one-electron states have been observed when electrons enter the QD from the thick barrier side [4]. We have used devices with symmetric barriers and, as discussed in the following, the conductance pattern at low bias can be attributed both to the ground states and to the excited states for N -electrons ($N \leq 6$). At larger voltage bias a crossover to a quasi continuum of excited states in the dot produces a huge resonant peak as in diodes which are not laterally confined.

The double barrier structures were grown by molecular beam epitaxy on n^+ GaAs substrate. The undoped active layers consist of a 5.1nm quantum well sandwiched between 5nm $Al_{0.33}Ga_{0.67}As$ barriers. Two 500nm GaAs layers, which are n -doped with Si to $10^{18}cm^{-3}$, provide the top and bottom contacts to the double barrier structure. The barriers are separated from the contacts by undoped spacer layers to prevent Si segregation in the QD. Circular pillars of radii varying between 50nm and $1\mu m$ were fabricated using electron-beam lithography and Ar/Cl_2 reactive ion etching. A polyimide planarisation patterning was used for the bonding pads [5].

Fig. 1a shows the I-V characteristics of diodes as a function of the lateral size, at a temperature of 4K. The voltage threshold shifts to higher bias when the radius decreases and the current density decreases as well. This reflects the growing influence of the lateral depletion length. In the following we will focus only on the experimental data collected on the smallest pillar whose radius is 100nm. A magnetic field is applied parallel to the current flow. Fig. 1b shows the I-V curves at $B = 0T$ and $9T$ at a temperature of 4K. A clear staircase-like structure appears in the low voltage bias region, whose last steps are poorly resolved because of the sharp increase of the current. Similar staircase structures have been widely reported by different groups and originate either from impurities or from QD's created by lateral confinement. Whenever a localized state is aligned with the emitter Fermi level, resonant tunneling is allowed and a plateau appears in the I-V characteristics. We argue in the following that, in our case, the plateaus are due to the discreteness of the N -electron states in the QD.

Fig. 2 shows the dynamical conductance dI/dV of the pillar as a function of the voltage bias at three temperatures ranging from $T = 1K$ to $T = 5K$. From the temperature dependence of all the peaks labeled by $\downarrow, \diamond, \square, \times$, and $+$ in the figure we conclude that they correspond to the tunneling of electrons through QD states at the emitter Fermi level. In fact, taking into account the intrinsic width of the QD states, we fit the width at half maximum of the first conductance peak by using the formula:

$$dI/dV \propto \int_{-\infty}^{+\infty} F(E - E_F) \frac{d}{dV} [T(E - \alpha V)] dE \quad (1)$$

where $F(E)$ is the Fermi distribution, E_F is the Fermi energy in the emitter, α is the energy-to-voltage conversion factor, and $T(E)$ is a transmission probability with a Lorentzian shape. As a result we extract $\alpha \simeq 0.31meV/mV$, which is in good agreement with the thickness of the barriers and the spacers. Moreover, using this value of α , we check that the LO-phonon replica is at about $36 \pm 5meV$ after the main resonance

peak (see fig. 1b). Thus, α is fairly constant over the whole bias range.

We performed magneto-tunneling measurements at $T = 35\text{mK}$ applying a magnetic field along the direction parallel to the current flow. Because the current has a sharp increase with the voltage close to the threshold, we cannot directly plot the conductance data for a quantitative analysis. In fig. 3 the derivative of the differential conductance, d^2I/dV^2 is depicted in a gray-scale graph. This has no direct physical interpretation by itself, but it emphasizes the peaks of the conductance. The maximum of a conductance peak is represented in this diagram by the boundary line between a clear band and a dark band, in increasing the bias. The contour lines represent the $dG/dV = 0\text{S.V}^{-1}$ values.

This diagram also reveals fluctuations of the Local Density of State (LDoS) of the emitter [6]. These fluctuations produce a fan-type pattern superimposed to the one due to the QD states, which becomes clearly visible at relatively high magnetic field. Indeed, for $B \geq 2T$, the LDoS fluctuations follow the behavior of the Landau levels in the emitter: the slope $\propto |dV|/dB$ of the fluctuations decreases with increasing B and corresponds to Landau levels which are deeply below the emitter Fermi level. We point out that their slope increases whenever a QD ground state is crossed. These slope changes are due to the progressive increase of the electron number in the QD. For $B \leq 2T$ the Landau levels are destroyed by disorder and the LDoS fluctuations are random. Although the LDoS fluctuations are clearly resolved, their current amplitude is weak compared to the one of the QD states and they produce very different features in the gray-scale plot. Thus, the two phenomena can be distinguished in almost the whole range of B and V .

We focus now on the six clearly resolved boundary lines of the gray-scale, which correspond to the peaks labeled by an arrow in fig 2. We attribute them to the N-electron ground states with $N=1,2,3,4,5$ and 6. Let us assume a parabolic lateral confining potential $V = \frac{1}{2}m^*\omega_0 r^2$ and put the first peak at $\sim 348\text{mV}$ in fig. 3 in correspondence with the single particle level $E_{0,0}$ of the Darwin-Fock spectrum [7] $E_{n,m} = \hbar\omega(2n + |m| + 1) + \frac{1}{2}m\hbar\omega_c$ (with $\omega = \sqrt{\omega_c^2/4 + \omega_0^2}$ and $\omega_c = eB/m^*$). Because we take $\alpha = 0.31\text{meV/mV}$, we obtain $\hbar\omega_0 = 9 \pm 1\text{meV}$. This corresponds to a radius $r \simeq \sqrt{2\hbar/m^*\omega_0} \simeq 15 \pm 1\text{nm}$. This is fairly larger than the expected radius of a single Si donor in GaAs, which is the most likely expected impurity in the quantum well region. On the contrary this value of the radius is in very good agreement with the one extracted from the calculation of the lateral confining potential in the pillar. This calculation consists in solving the Poisson equation in the Thomas-Fermi approximation for the electronic density in the contacts [8]. The resulting band profile enables us to determine the energy levels of the QD by solving numerically the Schrödinger

equation. The single particle energy spectrum that is obtained is very well approximated by an harmonic potential with $\hbar\omega_0 = 7 - 8\text{meV}$, and the calculated radius of the ground state is equal to $\simeq 17\text{nm}$.

Despite the fact that the barriers of our structures have the same thickness, we have strong evidence that the second conductance peak ($\sim 368\text{mV}$ in fig. 3) originates from Coulomb blockade. The simplest way to include interaction is to assume that the two electron ground state is given by $U_2^0 = 2E_{0,0} + E_C$. We define U_N^n as the n-th state of the N-electron spectrum, and E_C is the Coulomb interaction:

$$E_C = \int |\Psi(\mathbf{r}_1, \mathbf{r}_2)|^2 \frac{e^2}{4\pi\epsilon|\mathbf{r}_2 - \mathbf{r}_1|} d\mathbf{r}_1 d\mathbf{r}_2 \quad (2)$$

Since we measure the electro-chemical potential of the QD defined by $\mu(N) = U_N^0 - U_{N-1}^0$, we interpret the separation between the first and the second peak as E_C . There is a factor of two discrepancy, however, between the experimental value $E_C^{\text{exp}} = \alpha \cdot 20\text{mV} \simeq 6 - 7\text{meV}$ and the theoretical one estimated perturbatively from eq. 2 with single particle wavefunctions of the harmonic potential, $E_C^{\text{th}} = e^2 \sqrt{m^*\omega_0/32\pi\hbar\epsilon^2} \simeq 14\text{meV}$. This can be justified by taking into account the finite width of the QD as well as the screening of the electrons in the contacts. Following [4], we estimate the in plane separation of the electrons in the QD as 10nm, while the electrons in the contacts are at a distance $\lambda \simeq 13\text{nm}$ (including the screening length in the contacts $\simeq 8\text{nm}$). Therefore, the Coulomb integral should be cut off at separations $|\mathbf{r}_2 - \mathbf{r}_1| \geq \lambda$, what reduces the bare theoretical Coulomb interaction of our device to the expected value.

One more argument in favour of our interpretation is the observation that the separation between the two peaks increases slightly with B . Such an increase has already been observed [1] and is due to the squeezing of the electron orbits which causes an increase of E_C .

At $B = 0T$, the Darwin-Fock spectrum has degenerate sets of states separated by $\hbar\omega_0$, these shells being completely filled for $N = 2, 6, 12, \dots$. The degeneracy is completely lifted by the electron-electron interaction. We attribute the set of four lines in the voltage bias range $420\text{mV} - 460\text{mV}$ to the N-electron ground states with $N=3,4,5$ and 6 which fill progressively the second shell. Keeping α constant in the whole bias range, the experimental separation between the two shells is $\sim 15\text{meV}$, which is about $E_C + \hbar\omega_0$, as expected in the Constant Interaction (CI) model.

Fig. 4 is the result of an exact calculation of the energy spectrum of the QD using a Lanczos algorithm, assuming a parabolic potential and a Coulomb interaction ($\hbar\omega_0 = 8\text{meV}$, $E_C = 6\text{meV}$). The shell structure is clearly visible in $\mu(N)$, as well as the characteristic pairing of levels for particles with opposite spins. According to the CI model, the addition energy $\mu(N) - \mu(N - 1)$ for each even electron should always be E_C . However

E_C^{th} is reduced to 5meV in the second shell, because of correlation effects [9] and we measure an even smaller value $E_C^{exp} \simeq 3 - 4\text{meV}$ in this shell. Again, we attribute the difference between E_C^{th} and E_C^{exp} mainly to the fact that the assumption of the QD as isolated in the Lanczos calculation is unphysical. It ignores the coupling of the dot with the electrodes. The occupation rate for the $N \geq 4$ electron ground states appears to be noticeably less than that of the first ground states, what implies the observed reduction of the Coulomb blockade. Indeed, in the real device, any increase of V lowers the collector barrier height and increases the energy window through which the tunneling occurs, hence enhancing transport through excited states.

We conclude that there is a close correspondence between the solid lines of fig. 4 and the six main lines of the experimentally observed conductance diagram and attribute these to tunneling while the dot is in its N -electron ground state, with increasing N .

We claim that the additional temperature dependent features of the fig. 2, not discussed up to now, are due to the excited states of the N -electron spectra. Such separation of excited and ground states in a non-linear transport experiment implies that the collector barrier is slightly less transparent than the emitter one. This originates probably from fluctuations of the nominal parameters during the growth. This hypothesis is corroborated by the data in the negative bias, where the distinction between excited and ground states is not possible. These peaks appear to have a correspondence to analogous features in the calculated spectrum of fig. 4, lying between the first and the second shell. The \diamond , \square and \circ -dotted lines are respectively the first, second and third one-electron excited states corresponding to the $E_{0,-1}, E_{0,1}$ and $E_{0,-2}$ Darwin-Fock states. The \times line corresponds to the first excited 2 electrons state U_2^1 , with a total spin $S = 1$, referred to the single particle ground state energy U_1^0 (as all the U_2^n in the following). Note that the singlet-triplet transition ($U_2^0 - U_2^1$) occurs for $B \geq 9T$ and is not observed. The $+$ line describes the second 2-electrons excited state U_2^2 with $S = 0$. At $B = 0T$, $U_2^2 - U_2^0 = \hbar\omega_0$, so that we expect to observe the states in the following order when V increases: U_1^0 , U_2^0 , U_1^1 (which is 2-fold degenerate), U_2^1 , U_2^2 and U_1^2 .

In fig. 3 we have marked the experimental boundary lines that we attribute to these excited states. White symbols refer to lines that are clearly visible in our data. Black symbols indicate the expected position of these lines where the data are confused because of the LDoS fluctuations. Despite these uncertainties, the agreement between experimental and numerical results is satisfactory. We stress that, as in other experiments [4,10], the degeneracy of $E_{0,\pm 1}$ is lifted at $B = 0T$. This is a consequence of the lack of inversion symmetry of the Zinc Blende structure. Moreover the current contribution of the $E_{0,1}$ washes out quickly with B as expected from the

conservation of the angular momentum in 3D-0D tunneling [10,11].

Let us finally comment on the origin of the main resonance peak observed in the I-V curves (fig. 1b), like in large, non-laterally confined diodes involving tunneling through 2D states. Such a peak appears only if the momentum perpendicular to the interfaces is conserved during the tunneling. This is not the case for transport through a QD where only the energy is conserved. The only way to explain the shape of the I-V characteristics is to add a continuum of states which arises from the excited states of the QD.

In a simple non-interacting particles picture there are 12 levels for tunneling (including the 4 ground states of the second shell) when the chemical potential is twice $\hbar\omega_0$. As the Coulomb interaction suppresses the degeneracy, the mean level spacing is roughly $\simeq 1\text{meV}$ - which corresponds to our resolution in this experiment. The continuum becomes effective when $\mu \simeq 3\hbar\omega_0$ because of the 64 available states (including the 6 ground states of the third shell); as a consequence there is no way to observe excited levels beyond the second shell of our QD structure.

In conclusion, we have reported on non linear magnetotunneling experiment conductance measurements carried out in a single QD. Our data are consistent with the spectroscopy of few-electron states, even if LDoS fluctuations decrease the resolution of the experiment. We clearly observe a shell structure with a sizeable reduction of the Coulomb interaction in the second shell, probably due to screening. The first excited states for the one- and two-electron states can be identified. Finally we attribute the main I-V peak to the growing number of excited-states when the voltage bias is increased. Quantitative discrepancies with exact diagonalization of an isolated QD show that the role of the contacts in these non linear transport experiments cannot be ignored.

We would like to thank L. Couraud for his technical help, M. Boero, J.P. Holder and A.K. Savchenko for fruitful discussions. Work partly supported by INFM (Pra97-QTMD) and by EEC with TMR project, contract FMRX-CT98-0180.

-
- [1] L. P. Kouwenhoven, T. H. Oosterkamp, M. W. S. Danoesastro, M. Eto, D. G. Austing, T. Honda, and S. Tarucha, *Science* **278**, 1788 (1997); S. Tarucha, D.G. Austin, T. Honda, R.J. van der Hage and L.P. Kouwenhoven, *Phys. Rev. Lett.* **75**, 1996 (1995).
 - [2] T. Schmidt, M. Tewordt, R. H. Blick, R. J. Haug, D. Pfannkuche, K. v. Klitzing, A. Förster and H. Luth, *Phys. Rev. B* **51**, 5570 (1995);
 - [3] J.W. Sleight, E.S. Hornbeck, M.R. Deshpande,

M.A. Reed, R.G. Wheeler, R.C. Bowen, W.R. Frensley, J.N. Randall and R.J. Maryi Phys. Rev. B **53**, 15727 (1996);

- [4] Bo Su and V.J. Goldman, *Superlattices and Microstructures* **12**, 305 (1992);
- [5] G. Faini, H. Ramdane, F. Mollet and H. Launois, *Resonant tunneling in semiconductors: physics and applications*, L.L. Chang, E.E. Mendez, C. Tejedor eds. NATO ASI Series, Vol. (1991);
- [6] T. Schmidt, R. J. Haug, V.I. Fal'ko, K. v. Klitzing, A. Förster and H. Luth, Phys. Rev. Lett. **78**, 1540 (1997);
- [7] V. Fock, Z. Phys. **47**, 446 (1928).
- [8] Y. Galvão Gobato, J.M. Berroir, Y. Guldner, G. Faini and H. Launois, *Superlattices and Microstructures* **12**, 473 (1992);
- [9] A. Angelucci and A. Tagliacozzo, Phys. Rev. B **56**, R7088 (1997).
- [10] B. Jouault, J.P. Holder, M. Boero, G. Faini, F. Laruelle, E. Bedel, A.K. Savchenko and J.C. Inkson, condmat/9803232 (1998), to be published.
- [11] B. Jouault, M. Boero, G. Faini and J.C. Inkson, condmat/9809071 (1998), to be published.

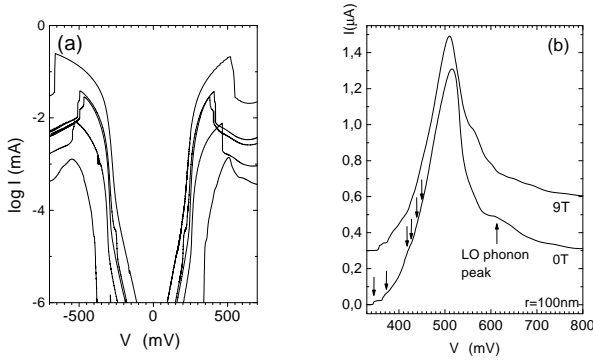


FIG. 1. (a) I-V curves at $T = 4K$ for different pillars: curves refer to increasing radii (100,200,300, 350 and 1000 nm), from bottom to top; (b) I-V curve of the smallest pillar ($r = 100nm$).

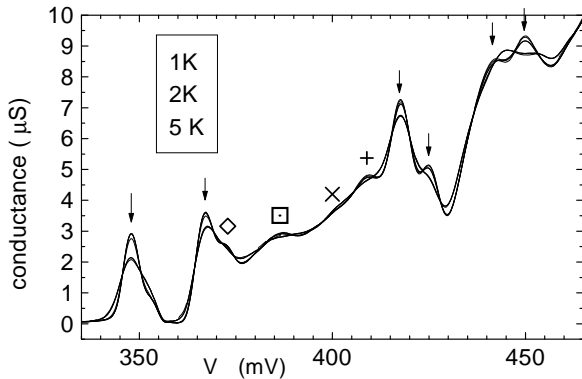


FIG. 2. Spectra of dI/dV vs V at $T = 1, 2$ and $5K$.

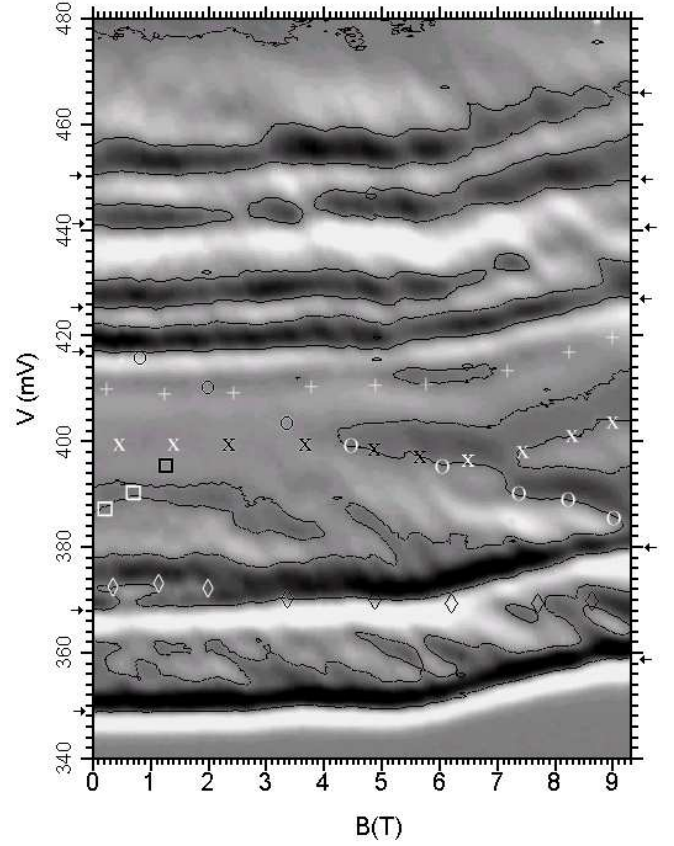


FIG. 3. Gray-scale plots of the derivative of the differential conductance $= d^2I/dV^2$, vs bias voltage and magnetic field (steps 0.1mV and 0.02T) numerically obtained from the measured $G(V)$ data. (white, $dG/dV \geq 5\mu S/mV$; black, $dG/dV \leq -5\mu S/mV$; $dG/dV = 0$ corresponds to the contour lines.

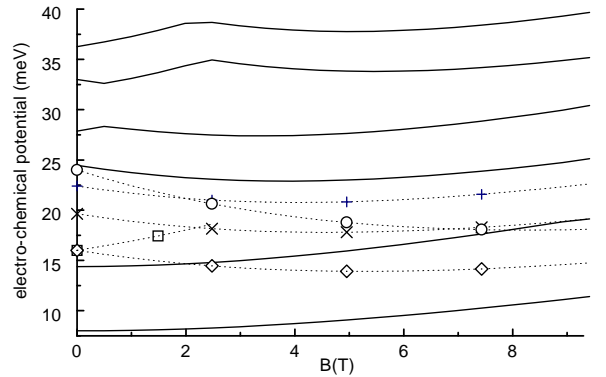


FIG. 4. Chemical potential $\mu(N)$ from the calculated energy spectrum. The solid lines correspond to the dot in the ground states with $N \leq 6$; the dotted lines correspond to the dot in the lowest excited states for electron occupancy $N = 1$ and 2 (see text for details).